medRxiv preprint doi: https://doi.org/10.1101/2020.05.21.20104521.this version posted May 22, 2020. The copyright holder for this preprint (which was not certified by peer review) is the author/funder, who has granted medRxiv a license to display the preprint in perpetuity. It is made available under a CC-BY-NC-ND 4.0 International license .

Full genome viral sequences inform patterns of SARS-CoV-2 spread into and within Israel

Danielle Miller[1*], Michael A. Martin[2,3*], Noam Harel[1*], Talia Kustin[1*], Omer Tirosh[1*], Moran Meir[1], Nadav Sorek[4], Shiraz Gefen-Halevi[5], Sharon Amit[5], Olesya Vorontsov[6], Dana Wolf[6], Avi Peretz[7,8], Yonat Shemer-Avni[9], Diana Roif-Kaminsky[10], Na'ama Kopelman[11,] Amit Huppert[12,13], Katia Koelle[2], Adi Stern[1,14]

[1] School of Molecular Cell Biology and Biotechnology, George S. Wise Faculty of Life Sciences, Tel Aviv University, Israel
[2] Department of Biology, Emory University, Atlanta, GA, USA
[3] Population Biology, Ecology, and Evolution Graduate Program, Laney Graduate School, Emory University, Atlanta, GA, USA
[4] Microbiology laboratory, Assuta Ashdod University-Affiliated Hospital. Ashdod, Israel
[5] Clinical Microbiology Laboratory, Sheba Medical Center, Ramat-Gan, Israel
[6] Clinical Virology Unit, Hadassah Hebrew University Medical Center, Jerusalem, Israel.
[7] The Azrieli Faculty of Medicine, Bar-Ilan University, Safed, Israel
[8] Clinical Microbiology Laboratory, The Baruch Padeh Medical Center, Poriya, Tiberias, Israel
[9] Clinical Virology Laboratory, Soroka Medical Center and the Faculty of Health Sciences, Ben-Gurion University of the Negev, Beer-Sheva, Israel
[10] Microbiology Division, Barzilai University Medical Center, Ashkelon, Israel
[11] Department of Computer Science, Holon Institute of Technology, Holon, Israel
[12] Bio-statistical and Bio-mathematical Unit, The Gertner Institute for Epidemiology and, Health Policy Research, Chaim Sheba Medical Center, Tel Hashomer, 52621 Israel
[13] School of Public Health, the Sackler Faculty of Medicine, Tel-Aviv University, Tel Aviv, 69978 Israel
[14] Edmond J. Safra Center for Bioinformatics at Tel Aviv University
* Co-equal authorship

ABSTRACT

Full genome sequences are increasingly used to track the geographic spread and transmission dynamics of viral pathogens. Here, with a focus on Israel, we sequenced 212 SARS-CoV-2 sequences and use them to perform a comprehensive analysis to trace the origins and spread of the virus. A phylogenetic analysis including thousands of globally sampled sequences allowed us to infer multiple independent introductions into Israel, followed by local transmission. Returning travelers from the U.S. contributed dramatically more to viral spread relative to their proportion in incoming infected travelers. Using phylodynamic analysis, we estimated that the basic reproduction number of the virus was initially around ~2.0-2.6, dropping by two-thirds following the implementation of social distancing measures. A comparison between reported and model-estimated case numbers indicated high levels of transmission heterogeneity in SARS-CoV-2 spread, with between 1-10% of infected individuals resulting in 80% of secondary infections. Overall, our findings underscore the ability of this virus to efficiently transmit between and within countries, as well as demonstrate the effectiveness of social distancing measures for reducing its spread.

NOTE: This preprint reports new research that has not been certified by peer review and should not be used to guide clinical practice.

medRxiv preprint doi: https://doi.org/10.1101/2020.05.21.20104521.this version posted May 22, 2020. The copyright holder for this preprint (which was not certified by peer review) is the author/funder, who has granted medRxiv a license to display the preprint in perpetuity. It is made available under a CC-BY-NC-ND 4.0 International license .

INTRODUCTION

In December 2019 an outbreak of severe respiratory disease was identified in Wuhan, China (Huang, et al. 2020). Shortly later, the etiological agent of the disease was identified as severe acute respiratory syndrome coronavirus 2 (SARS-CoV-2) (Zhou, et al. 2020; Zhu, et al. 2020), and the disease caused by the virus was named coronavirus disease 19 (COVID-19). The virus has since spread rapidly across the globe, causing a WHO-declared pandemic with social and economic devastation in many regions of the world. The infectious disease research community has quickly stepped up to the task of characterizing the virus and its replication dynamics, describing its pathogenesis, and tracking its movement through the human population. Parameterized epidemiological models have been particularly informative of how this virus has spread with and without control measures in place (e.g., Tian, et al. 2020), and have been used to project viral spread both in the short-term (Flaxman, et al. 2020) and in the more distant future (Kissler, et al. 2020).

Along with epidemiological analysis based on case reports and COVID-19 death data, sequencing of viral genomes has become a powerful tool in understanding and tracking the dynamics of infections (Volz, et al. 2013; Gardy and Loman 2018). So-called "genomic epidemiology" allows for effective reconstruction of viral geographical spread as well as estimation of key epidemiological quantities such as the basic reproduction number of a virus, its growth rate and doubling time, and patterns of disease incidence and prevalence. Such insights have been used to inform policy makers during various pathogen outbreaks, as occurred for example in the 2014-2016 outbreak of Ebola virus in West Africa (Khoury, et al. 2018; Armstrong, et al. 2019), and during this current SARS-CoV-2 pandemic (Bedford, et al. 2020; Fauver, et al. 2020).

Here, we set out to sequence SARS-CoV-2 from samples across the state of Israel, with the aim of gaining a better understanding of introductions of the virus into Israel, spread of the virus inside the country, and the epidemiology of the disease, including (a) the basic reproduction number of the virus before and after social distancing measures were implemented, and (b) the extent of viral superspreading within Israel. We sought to gain this understanding within the context of existing epidemiological knowledge, including that the first confirmed cases of SARS-CoV-2 infection in Israel were reported in early-February, followed by many identified SARS-CoV-2 cases in travelers returning to Israel mainly from Europe and the United States. Growth in the number of verified cases rapidly ensued, which led to increased measures of social distancing, including the cessation of passenger flights to Israel, school closure, and eventually a near complete lockdown across the entire state of Israel. Quarantining of returning travelers from Europe was implemented between February 26 and March 4, 2020, and subsequently all incoming travel to Israel was arrested on March 9. In the meantime, the rate of testing was ramped up, eventually reaching a rate of more than 1,500 tests per million people per day. The reported daily incidence and reported numbers of daily severe cases peaked around mid-April and have dropped steadily since then. Despite this knowledge, many questions remain: Which of the multiple SARS-CoV-2 introductions resulted in sustained local transmission? How did the virus spread across the state? What was the magnitude of the virus's reproduction potential within Israel, and to what extent did control measures mitigate its spread? Here, through a comprehensive set of phylogenetic and phylodynamic analyses, we quantitatively address these questions.

medRxiv preprint doi: https://doi.org/10.1101/2020.05.21.20104521.this version posted May 22, 2020. The copyright holder for this preprint (which was not certified by peer review) is the author/funder, who has granted medRxiv a license to display the preprint in perpetuity. It is made available under a CC-BY-NC-ND 4.0 International license .

RESULTS & DISCUSSION

In order to gain a better understanding of the dynamics of SARS-CoV-2 spread into and within Israel, we sequenced the virus from a cohort of patients representing a random sample across Israel, resulting in 212 full-genome SARS-CoV-2 sequences (Methods). A total of 224 unique single nucleotide variants (SNVs) were identified between the Wuhan reference sequence and this set of sequences from Israel. Figure 1 shows the distribution of identified SNVs along the genome and their counts in the sequenced samples. Of these SNVs, 141 were non-synonymous, 72 were synonymous, and the remaining 11 were in non-coding regions. One of the most abundantly detected SNVs was a non-synonymous variant D614G found in the spike protein, which was present in 90% of the sequences. This variant has generated much interest as it has been reported to potentially increase the transmissibility of the virus (Korber, et al. 2020). Of note however, the alternative hypothesis that the observed increases in this variant's frequency is due to demographic considerations and genetic drift has not been ruled out.

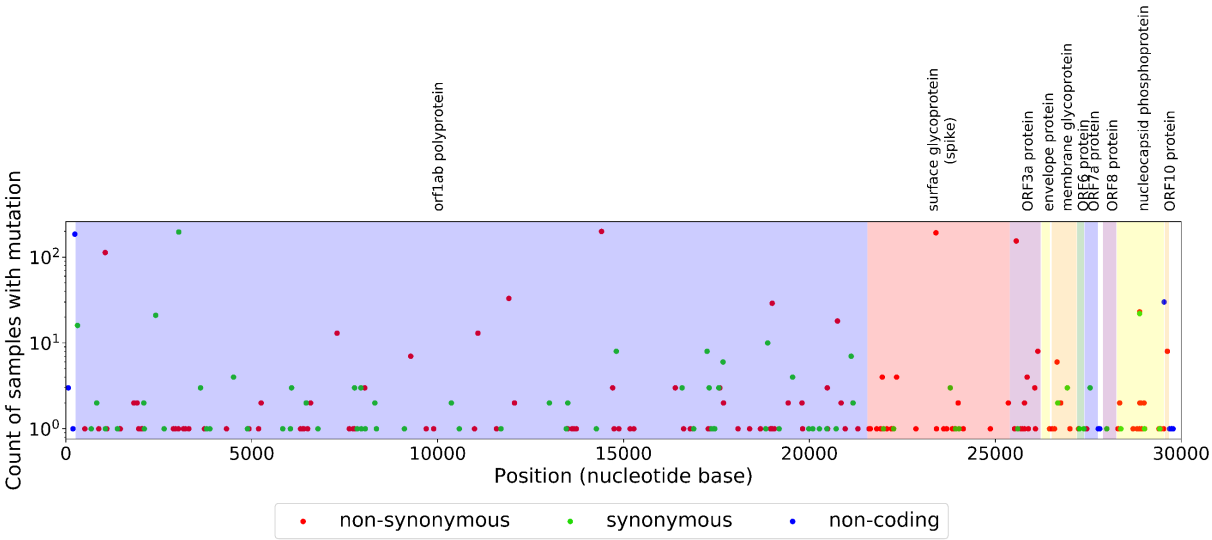

Figure 1. Variation found in sequenced samples from Israel. Counts of identified SNVs across the SARS-CoV-2 genome.

We also found five different high confidence genomic deletions, spanning between one and eighteen nucleotides (Fig. 2) (Methods), each of which was found in one to two samples. Three of these five deletions occurred in multiples of three and were in-frame deletions or affected non-coding regions. Of the remaining two deletions, deletion #3 spanned ten nucleotides, and likely prevents the translation of ORF7a. Deletion #4 occurred at the end of ORF8 and causes the replacement of the last amino acid with an additional five amino acids. Notably, an 81 nt in-frame deletion in ORF7a has been previously reported (Holland, et al. 2020), as has been a 382 nt deletion in ORF8 (Su, et al. 2020), suggesting that the virus is to some extent tolerant to deletions in these ORFs.

medRxiv preprint doi: https://doi.org/10.1101/2020.05.21.20104521.this version posted May 22, 2020. The copyright holder for this preprint (which was not certified by peer review) is the author/funder, who has granted medRxiv a license to display the preprint in perpetuity. It is made available under a CC-BY-NC-ND 4.0 International license .

(A)

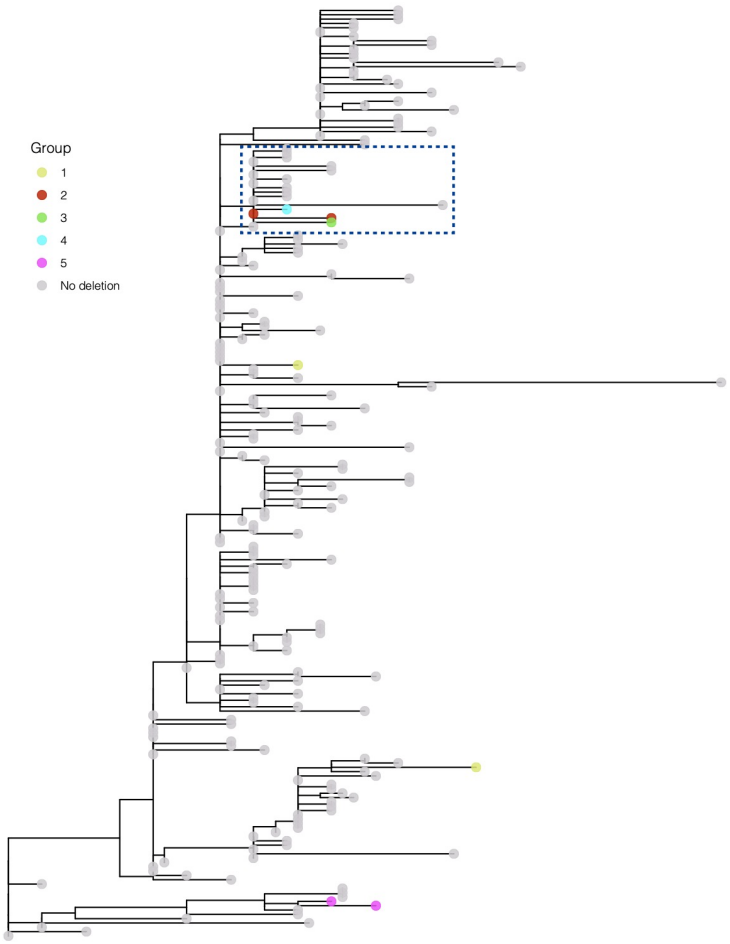

(B)

#	Genome coordinates	Length	ORF/Genomic location	Suggested effect	Number of samples found in	Sample IDs	Number of reads supporting deletion
1	686-694	9nt	ORF1ab polyprotein	Deletion of 3 amino acids	2	2086008, 130710157	3575, 1852
2	3882-3899	18nt	ORF1ab polyprotein	Deletion of 6 amino acids and an additional single amino acid mutation	2	2089839, 2089852	427, 605
3	27387-27396	10nt	End of ORF6 and start of ORF7a	Stop codon of ORF6 is recreated. Start codon of ORF7a is deleted with no in-frame replacement	1	13077726	3801
4	28254	1nt	End of ORF8	Last amino acid is replaced by a 5 amino acid addition	1	2086033	2849
5	29746-29748	3nt	3' UTR	Non-coding, unknown	2	51137844, 51141225	42,147

Figure 2. Deletions found in Israeli samples. (A) Maximum-likelihood tree of Israeli sequences highlighting sequences found with deletions that are color-coded and described in (B). A clade with three independent deletions occurring in four samples is boxed. The phylogeny displayed was created with the ggtree package (Yu, et al. 2017).

medRxiv preprint doi: https://doi.org/10.1101/2020.05.21.20104521.this version posted May 22, 2020. The copyright holder for this preprint (which was not certified by peer review) is the author/funder, who has granted medRxiv a license to display the preprint in perpetuity. It is made available under a CC-BY-NC-ND 4.0 International license .

When focusing on deletions that occurred in two samples, we noted that the two samples bearing deletion #1 were located in very remote clades on the phylogeny, suggesting that the deletion occurred two independent times. Deletion #5 on the other hand was present in two related samples that were sampled five days apart from each other. Deletions #2, #3 and #4 revealed an intriguing pattern: three independent deletions (one of which was present in two samples) were all part of the same clade that included eighteen samples (Fig. 2). One non-synonymous SNV defined this clade: S2430R in ORF1b which affects the non-structural protein NSP16. This protein has been reported to be a 2'O-methyl-transferase that enhances evasion of the innate immune system (Menachery, et al. 2014).

While further in-depth investigation of SARS-CoV-2 indels is clearly needed, at this point we conjecture that the deletions we detected are neutral or to some extent deleterious, and that deletions in SARS-CoV-2 are likely to occur frequently given the number of deletions detected in our samples.

Origins and transmission patterns in Israel

We next set out to explore patterns of SARS-CoV-2 introduction into Israel. Figure 3 shows the time-resolved phylogeny inferred using the 214 Israeli sequences (212 sequenced here and two additional ones sequenced previously) in addition to 4,693 representative sequences from across the world. This phylogeny allowed us to characterize the major viral clades circulating within Israel and to infer the geographic sources and timing of virus introductions into the state. We found multiple introductions into Israel from both the U.S and Europe, the latter including mainly the U.K., France and Belgium. Over 70% of the clade introductions into Israel (confidence intervals ranging from ~50% to ~80%, see Methods) were inferred to have occurred from the U.S., while the remaining were mainly from Europe. During the entire epidemic in Israel, very close monitoring of all incoming infected travelers was imposed, and reports show that only ~27% of infected returning travelers were from the U.S. The discrepancy between these estimated proportions suggests that the travelers returning from the U.S. contributed substantially more to the spread of the virus in Israel than would be proportionally expected. This may have occurred due to the gap in policy that allowed returning non-European travelers to avoid quarantine until March 9, or due to different contact patterns of those who returned from the U.S. Moreover, this suggests that had flights from the U.S. been arrested at the same time that flights from Europe were arrested (between February 26 and March 4, instead of by March 9), a substantial fraction of the transmission chains in Israel would have been prevented.

medRxiv preprint doi: https://doi.org/10.1101/2020.05.21.20104521.this version posted May 22, 2020. The copyright holder for this preprint (which was not certified by peer review) is the author/funder, who has granted medRxiv a license to display the preprint in perpetuity. It is made available under a CC-BY-NC-ND 4.0 International license .

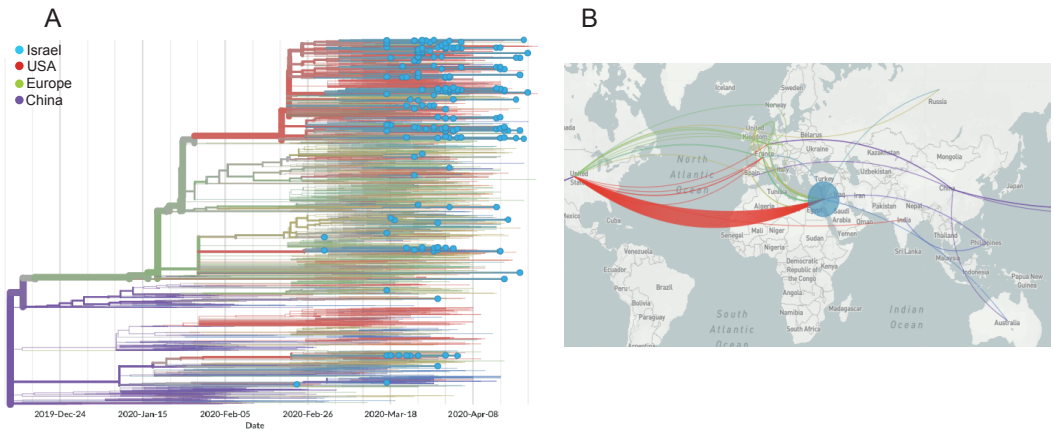

Figure 3. Patterns of SARS-CoV-2 introduction into Israel. (A) Time-resolved phylogeny inferred using viral sequences from Israel (blue tips) and around the world (tips without dots). Lineages are colored by inferred region of circulation. Phylogeographic analysis reveals multiple introductions into Israel, mainly from the U.S. (B) Map of phylogenetically inferred introductions into Israel highlighting the dominance of the U.S. and to a lesser extent Europe as the geographic sources of SARS-CoV-2 introductions into Israel. Figures generated using NextStrain (Hadfield, et al. 2018).

As the pandemic spread, entry into Israel was restricted, and local transmissions became dominant. Transmission patterns into and between six various geographical regions in Israel (North district, Tel Aviv district, South coast district, Jerusalem district, and South district) are shown in Figure 4. While most local transmission occurred inside defined regions, transmission among distinct regions was also observed, such as, for example, movement between Jerusalem and the north district of Israel.

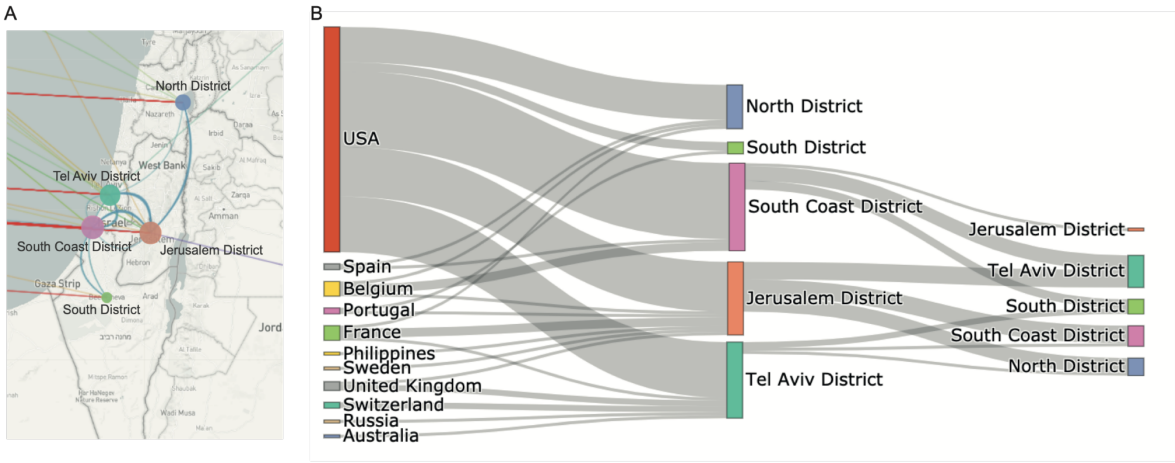

Figure 4. Spread of SARS-CoV-2 into and within Israel. (A) Map of Israel with geographic locations of samples, and inferred spread into Israel (colored lines) and inside Israel (blue lines). (B) Alternative view of spread into and inside Israel. Each line represents a transmission event inferred based on the phylogeny. Thicker lines indicate multiple transmission events.

medRxiv preprint doi: https://doi.org/10.1101/2020.05.21.20104521.this version posted May 22, 2020. The copyright holder for this preprint (which was not certified by peer review) is the author/funder, who has granted medRxiv a license to display the preprint in perpetuity. It is made available under a CC-BY-NC-ND 4.0 International license .

Phylodynamic modeling of viral spread in Israel

To estimate the basic reproduction number of SARS-CoV-2 in Israel initially and then following the implementation of social distancing measures, we performed coalescent-based phylodynamic inference using PhyDyn (Methods). We note that existing phylodynamic analyses of SARS-CoV-2 have shown that the effective reproduction number R_E of the virus has decreased over time, as quarantine and social distancing measures have been implemented within specific regions (Danesh, et al. 2020; Vaughan, et al. 2020; Volz, Baguelin, et al. 2020). However, many of these analyses have to date modeled reductions in R_E as stemming from the depletion of susceptible individuals (Volz, Baguelin, et al. 2020), rather than from reductions in R_0, the latter of which would be consistent with lowering of contact rates. Other analyses, particularly those that use the birth-death model approach for phylodynamic inference, have allowed for changes in R_0 over time (Danesh, et al. 2020; Vaughan, et al. 2020), but cannot as easily accommodate structure in the infected host population (e.g., that some individuals are exposed but not yet infectious, and that transmission heterogeneity exists between infected individuals). Our phylodynamic analysis here, based heavily on existing coalescent-based model structures that have been applied to SARS-CoV-2 (Volz 2020), instead allows for this structure to be accommodated and for R_0 to change in a piecewise fashion over time.

Our phylodynamic analysis assumes an underlying susceptible-exposed-infected-recovered (SEIR) epidemiological model for SARS-CoV-2 transmission dynamics and explicitly incorporates transmission heterogeneity (Methods). Recent epidemiological analyses have estimated considerable levels of SARS-CoV-2 transmission heterogeneity, with ~7-10% of infected individuals estimated to be responsible for 80% of secondary infections (Bi, et al. 2020; Endo, et al. 2020). Instead of assuming a given level of transmission heterogeneity for Israel, we instead performed phylodynamic inference of the SEIR model across a range of transmission heterogeneities ranging from p_h = 1% to 20% of infected individuals being responsible for 80% of secondary infections. We estimated R_0 prior to March 19 to be approximately 2.0 across this superspreading range, with estimates increasing towards R_0 = 2.4 to 2.6 at extremely high levels of superspreading (p_h = 1-2%) (Figure 5A). Across this superspreading range, we robustly estimated that quarantine measures had the effect of reducing R_0 by approximately two-thirds (α = ~30%; Figure 5B; see Table S2 for model parameter priors and estimated values).

Figure 5C shows the cumulative number of SARS-CoV-2 cases by April 22, estimated by our phylodynamic analyses across the considered superspreading range. Estimates of the cumulative number of cases is highly sensitive to the level of assumed transmission heterogeneity, particularly at high levels of superspreading (p_h = 1-5%). Comparison between these inferred cumulative cases and reported case numbers (dotted line in Figure 5C) indicates that SARS-CoV-2 transmission dynamics were driven by an extremely high level of viral superspreading. Specifically, if we assume almost complete case reporting, our phylodynamic analysis indicates that between 5-9% of infections are responsible for 80% of secondary infections; with lower assumed levels of case reporting, between 1-5% of infections would be responsible for this 80% of secondary infections.

medRxiv preprint doi: https://doi.org/10.1101/2020.05.21.20104521.this version posted May 22, 2020. The copyright holder for this preprint (which was not certified by peer review) is the author/funder, who has granted medRxiv a license to display the preprint in perpetuity. It is made available under a CC-BY-NC-ND 4.0 International license .

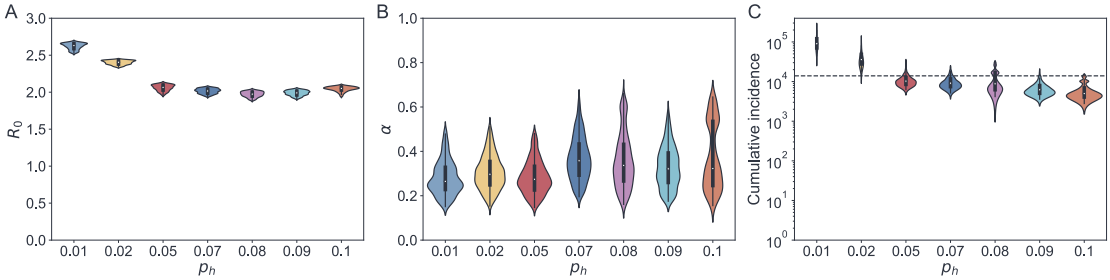

Figure 5. Estimated epidemiological parameters across different levels of transmission heterogeneity. The parameter p_h gives the fraction of infected individuals that are responsible for P = 80% of secondary infections. Higher p_h values correspond to less transmission heterogeneity. (A) Estimated R_0 in Israel prior to March 19, 2020. (B) Estimated fraction by which R_0 in Israel changed after March 19. (C) Estimated cumulative number of infected individuals in Israel on the date of the last sampled sequence (April 22, 2020). An infected individual is assumed to contribute to cumulative incidence at the end of their infectious period. Horizontal dotted line at N = 13,942 shows the cumulative number of reported cases on April 22, 2020 as given by the ECDC (https://opendata.ecdc.europa.eu/covid19/casedistribution/csv). In (A)-(C), only values that fall within the 95% highest posterior density intervals are shown.

Phylodynamic analysis further allows us to visualize inferred epidemiological dynamics. In Figure 6, we show inferred patterns of prevalence (Fig. 6A) and incidence (Fig. 6B) for three different assumed levels of viral superspreading. Inferred patterns of prevalence corroborate epidemiological findings that the number of cases started to decline in early April. Inferred patterns of cumulative incidence indicate that reporting rates were initially low, but improved considerably over the time course of viral spread. The 'leveling off' of cumulative incidence around late March/early April observed in both the reported case data and in our inferred epidemiological dynamics, ground-truthing the results of our phylodynamic analyses.

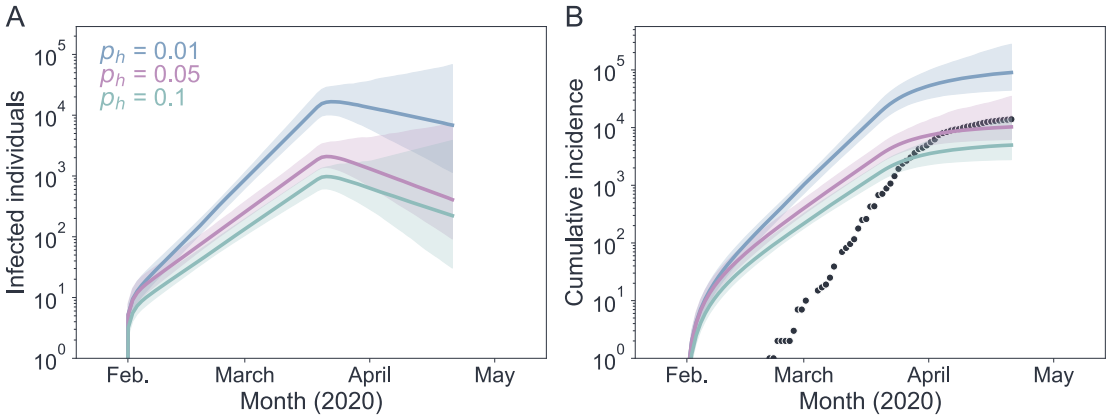

Figure 6. Epidemiological dynamics inferred using phylodynamic analysis. (A) Estimated number of currently infected individuals (I_l + I_h) over time. (B) Estimated cumulative number of infected individuals. An infected individual is assumed to contribute to cumulative incidence at the end of their infectious period. Black dots show the cumulative number of reported cases in Israel over time, as given by the ECDC. Model-predicted numbers of infected individuals include both classes of infected individuals (I_l + I_h). In (A) and (B), lines show median estimates of models with different levels of transmission heterogeneity: p_h = 0.01 (blue), 0.05 (pink), and 0.10 (green). Shaded regions show the 95% highest posterior density.

medRxiv preprint doi: https://doi.org/10.1101/2020.05.21.20104521.this version posted May 22, 2020. The copyright holder for this preprint (which was not certified by peer review) is the author/funder, who has granted medRxiv a license to display the preprint in perpetuity. It is made available under a CC-BY-NC-ND 4.0 International license .

Conclusions

Overall, our findings highlight the use of genomic data to effectively track the spread of an emerging virus using phylogenetic and phylodynamic approaches that have been developed to study viral outbreaks. We have hereby succeeded in tracking the main transmission chains that led to SARS-CoV-2 spread in Israel, and applied phylodynamic analysis to infer key epidemiological parameters governing its spread. Our results suggest that superspreading events are a main feature of SARS-CoV-2 spread, suggesting that focused measures to reduce contacts of select individuals/social events could dramatically mitigate viral spread. Finally our results highlight how global connectivity allows for massive introductions of a virus, and emphasize how border control and shelter-in-place restrictions are crucial for halting viral spread.

medRxiv preprint doi: https://doi.org/10.1101/2020.05.21.20104521.this version posted May 22, 2020. The copyright holder for this preprint (which was not certified by peer review) is the author/funder, who has granted medRxiv a license to display the preprint in perpetuity. It is made available under a CC-BY-NC-ND 4.0 International license .

METHODS

Ethics statement

An exemption from institutional review board approval was determined by the Israeli Ministry of Health as part of an active epidemiological investigation, based on use of anonymous data only and no medical intervention. The study was further approved by the Tel-Aviv University ethics committee (approval 0001274-1).

Details of samples & virus genome sequencing

With the aim of generating a random sample of viral infections across the entire country, a total of 213 samples were retrieved from six major hospitals in Israel spanning the entire geography of Israel from south to north (Table 1, Table S1).

We obtained RNA extracted from nasopharyngeal samples. Sequencing was performed based on the V3 Arctic protocol (https://artic .network/ncov-2019). Briefly, reverse transcription and multiplex PCR of 109 amplicons was performed, and adapters were ligated to allow for sequencing. All samples were run on an Illumina Miseq using 250-cycle V2 kits in the Technion Genome Center (Israel).

Determining genome consensus sequences

Sequencing reads were trimmed using pTrimmer, a multiplexing primer trimming tool (Zhang, et al. 2019), and then aligned to the reference genome of the SARS-CoV-2 (GenBank ID MN908947) using our AccuNGS pipeline (Gelbart, et al. 2019), which is based on BLAST (Altschul, et al. 1997), using an e-value of 10^{-9}. The pipeline allows for consensus determination and variant calling. We considered substitutions at the consensus sequence (as compared to the reference) only if a given base was present in 80% of the aligned reads, and five or more reads aligned to the reference; bases where the majority of reads showed a substitution but that did not fulfill these two conditions were deemed uncertain. Similarly positions to which no reads were mapped were also deemed uncertain, and such positions were assigned with an “N”. All deletions were manually verified: (a) over 98% of the reads covering the deletion site mapped to both ends of the deletion (i.e, bore evidence of the deletions), (b) the deletion was based on over 40 independent reads (on average >1,000 reads), and (c) coverage was high at both ends of the deleted region. Only sequences that spanned 90% of the reference genome were retained, leading to the removal of one sequence (Table S1), and hence a new set of 212 Israeli sequences was generated here. Another two Israeli sequences already available on GISAID were added to the phylogenetic analysis, leading to a total of 214 sequences from Israel.

The collection dates of the 214 Israeli sequences used in our analysis ranged from February 23 through April 22, 2020. The number of sequences is thus approximately 1.5% of the total number of reported cases on April 22.

medRxiv preprint doi: https://doi.org/10.1101/2020.05.21.20104521.this version posted May 22, 2020. The copyright holder for this preprint (which was not certified by peer review) is the author/funder, who has granted medRxiv a license to display the preprint in perpetuity. It is made available under a CC-BY-NC-ND 4.0 International license .

Table 1. General statistics on samples collected and sequenced.

	Age group	Number of samples	
Age group	0-9	8	
	10-19	17	
	20-29	42	
	30-39	28	
	40-49	26	
	50-59	29	
	60-69	31	
	70-79	15	
	80-89	11	
	90 and up	3	
	unknown	2	
Location and hospital	**Hospital**	**City**	**Number of samples**
	Barzilai Medical Center	South coast district	30
	Samson Assuta Ashdod University Hospital	South coast district	23
	Hadassah University Hospital - Ein Kerem	Jerusalem district	62
	Poria Medical Center	North district	26
	Sheba Medical Center	Tel Aviv district	51
	Soroka Medical Center	South district	20
Sex		**Number of samples**	
	Female	101	
	Male	111	

Phylogenetic analyses

All available full-length SARS-CoV-2 genomes from outside of Israel (a total of 16,403 sequences) were retrieved from GISAID on May 5, 2020. All sequences from a non-human host as well as sequences with incomplete sampling date (YYYY-MM or YYYY-MM-XX) or a high level of uncertainty (>10% ambiguous bases marked as N) were removed. All available sequences were then down-sampled to 4,693 representative sequences across the globe using the latest build of NextStrain ncov pipeline (Hadfield, et al. 2018; Hadfield, et al. 2019) (https://github.com/nextstrain/ncov). 1195 of these 4,693 sequences were from the U.S., while 1991 were from Europe. The 212 new Israeli sequences were added to the tree.

Confidence in numbers and fractions of importation events

Confidence in the relative number of importation events from the U.S. vs. Europe was assessed using two measures of confidence intervals, which were aimed at testing whether the set of exogenous sequences was biased, or whether the set of Israeli sequences was biased. First, we generated 1,000 samples of the exogenous (non-Israeli) sequences using a bootstrap approach and assessed the fraction of importation events in each sample. Second, we similarly bootstrapped the local (Israeli) sequences only and assessed the fraction of importation events in each sample. The reported confidence interval includes the lower bound and higher bound of both bootstrapping schemes.

medRxiv preprint doi: https://doi.org/10.1101/2020.05.21.20104521.this version posted May 22, 2020. The copyright holder for this preprint (which was not certified by peer review) is the author/funder, who has granted medRxiv a license to display the preprint in perpetuity. It is made available under a CC-BY-NC-ND 4.0 International license .

Down-sampling of global tree for phylodynamic analysis

Following the initial sampling of the global tree described above, we applied a second sampling specifically for the phylodynamic analysis. The down-sampling followed the recommended guidelines described previously for SARS-CoV-2 (Volz, Boyd, et al. 2020). We used two sampling techniques:

(i) *Random time stratified sampling* – we sampled a total of 100 sequences from outside of Israel across ν=5 time intervals such that each time interval contained approximately 20 sequences.

(ii) *Closest sequence match* – we will define S_{ISR} as the set of all sequences from Israel. We sample the exogenous set of sequences from the global tree with the minimal cophenetic distance between each Israeli sequence belonging to S_{ISR} as based on the maximum likelihood phylogeny. This allow including sequences closely related to sequences from Israel.

We next manually curated the sequences from Israel to ensure they represent a random sample across Israel. To this end we removed samples suspected to be from the same household, samples with consecutive identifiers, or identical samples with similar identifiers and similar dates. Only one sample from a given household was chosen randomly. This led to a removal of 6 sequences.

Following down-sampling and manual curation, a phylogenetic tree was inferred using the NextStrain pipeline (Hadfield, et al. 2018). The tree topology was validated as a legitimate representative of the global tree by performing 1,000 random samples containing 373 sequences from the global tree. The Kendall-Colijn metric (Kendall and Colijn 2016) was used to assess distance between each random sample and the original tree, allowing us to create a null distribution. The λ parameter, which determines the trade-off between topology and branch length, was set to zero, thus accounting for the tree topology alone. The significance of down-sampling procedure was thus obtained by comparing the Kendall-Colijn metric of the down-sampled tree to the null distribution.

Rate of importations

As described previously, strong global connectivity can result in a high number of independent seeding events (Chinazzi, et al. 2020), and we thus aimed at generating the distribution of importation dates (Volz, Boyd, et al. 2020). This was achieved based on the time-resolved phylogeny, which was then used to estimate the date of initial importation as well as the date on which the rate of new importations dropped. Given a down sampled ML tree T^{ML}, we re-estimate a forest of trees using IQ Tree (Nguyen, et al. 2015) $\{T_1^{ML}, \dots, T_n^{ML}\}$ such that each tree T_i^{ML} is generated by randomly resolving polytomies in T^{ML}. Each T_i^{ML} is used to produce a time-based tree, T_i^{time} using TreeTime (Sagulenko, et al. 2018) with molecular clock rate $r \sim U[0.0009 - 0.0015\ ]$ substitutions/site/year. We deduce the distribution of all seeding events by taking the mid-branch date for each node leading to an Israeli tip for all trees. Both IQ Tree and TreeTime were executed using the Augur python package.

Phylodynamic Analysis

Phylodynamic analyses were conducted using BEAST2 v2.6.2 (Bouckaert, et al. 2019) and PhyDyn v1.3.6 (Volz and Siveroni 2018). An HKY substitution model with a lognormal prior for κ with mean log(κ) = 1.0 and standard deviation of log(κ) = 1.25 was used. We assumed no sites to be invariant and used an exponential prior for γ with a mean of 1.0. A strict molecular clock with a uniform prior between 0.0007 and 0.002 substitutions/site/year was

medRxiv preprint doi: https://doi.org/10.1101/2020.05.21.20104521.this version posted May 22, 2020. The copyright holder for this preprint (which was not certified by peer review) is the author/funder, who has granted medRxiv a license to display the preprint in perpetuity. It is made available under a CC-BY-NC-ND 4.0 International license .

used. A uniform prior was used for nucleotide frequencies. The down-sampled maximum likelihood tree generated using IQ Tree was used as a starting tree.

PhyDyn is a coalescent-based inference approach implemented in BEAST2, allowing for the integration over phylogenetic uncertainty (Volz 2012; Volz and Siveroni 2018). The program requires specification of an underlying epidemiological model, as well as any priors on parameters that will be estimated. In line with recent analyses (sarscov2.phylodynamics.org), we assumed that the epidemiological dynamics of SARS-CoV-2 were governed by Susceptible-Exposed-Infected-Recovered (*SEIR*) dynamics. Transmission heterogeneity has previously been described for viral pathogens including SARS-CoV-1 (Lloyd-Smith, et al. 2005) and appears to be important in the transmission dynamics of SARS-CoV-2 (Bi, et al. 2020; Endo, et al. 2020). To account for the possibility of transmission heterogeneity, as in previous work (sarscov2.phylodynamics.org), we modeled two classes of infected individuals: one with low transmissibility I_l and one with high transmissibility I_h. Mathematically, the epidemiological model is given by

$$dS/dt = -\beta_l I_l (S/N) - \beta_h I_h (S/N)$$
$$dE/dt = \beta_l I_l \left(\frac{S}{N}\right) + \beta_h I_h \left(\frac{S}{N}\right) - \gamma_E E$$
$$dI_l/dt = (1 - p_h)\gamma_E E - \gamma_I I_l$$
$$dI_h/dt = p_h \gamma_E E - \gamma_I I_h$$
$$dR/dt = \gamma_I I_l + \gamma_I I_h$$

We set as fixed the host population size to the population size of Israel, according to the European Centre for Disease Prevention and Control (N = 8,883,800), the average duration of time an individual spends in the exposed class ($1/\gamma_E$ = 3 days), and the average duration of time an individual spends in the infected (infectious) class ($1/\gamma_I$ = 5.5 days). These rates are based on a study that inferred transmissibility over the course of infection based on data from established SARS-CoV-2 transmission pairs (He, et al. 2020). R_0 in this model is given by $(\beta_h p_h + \beta_l(1 - p_h))/\gamma_I$, where p_h is the fraction of exposed individuals who transition to the I_h class. Instead of independently parameterizing β_h and β_l, we defined (as in previous work) the relative transmissibility of infected individuals in the I_h and I_l classes by the parameter $\tau = \beta_h/\beta_l$. We defined a parameter P as the fraction of secondary infections that were caused by a fraction p_h of the most transmissible infected individuals and set P to 0.8. Based on set values of P and p_h, we calculated τ as $(\frac{1-p_h}{p_h})/(\frac{1}{P} - 1)$. As such, we could easily parameterize the model across various levels of transmission heterogeneity, with a fraction p_h of infected individuals being responsible for 80% of secondary infections. Existing epidemiological analysis indicate that p_h is on the order of 7-10% (Bi, et al. 2020; Endo, et al. 2020) indicative of even more transmission heterogeneity than given by the 20/80 rule (Woolhouse et al., PNAS, 1997). We focused on the range of p_h between 1-10% in our phylodynamic analyses.

Again based on existing analyses (sarscov2.phylodynamics.org), we included an external reservoir, Y, in our analysis to allow for multiple introduced clades into Israel to be jointly considered. We assume symmetric migration of individuals in the E, I_l, and I_h classes in and out of Israel based on a per capita migration rate η. An exponential prior with a mean of 10 and an upper limit of 10 was used for η. Based on the results of the importation analysis described above, we assumed that the migration rate decreased to 25% of its original value after March 20, 2020. As migration is assumed to be symmetrical in and out of Israel it does not affect the focal *SEIR* model dynamics, however, it influences the probability that a given lineage's geographic state is assigned to Israel. We fix the rate of removal of individuals from

medRxiv preprint doi: https://doi.org/10.1101/2020.05.21.20104521.this version posted May 22, 2020. The copyright holder for this preprint (which was not certified by peer review) is the author/funder, who has granted medRxiv a license to display the preprint in perpetuity. It is made available under a CC-BY-NC-ND 4.0 International license .

Y to be $1/(1/\gamma_E + 1/\gamma_I)$ and estimate the rate of entry into *Y*, ρ, using a lognormal distribution with mean log(ρ) = 3.6 and standard deviation log(ρ) = 1.

In our model, we estimated a piecewise R_0 by estimating an initial R_0 that was in effect until March 19, 2020 slightly after strong social distancing measures were implemented, along with a factor α by which R_0 changed on March 19. We set the prior on R_0 to a lognormal distribution with mean log (R_0) of 1.5 and standard deviation of log (R_0) of 0.5. We set the prior on α to be uniform between 0 and 2, thereby allowing R_0 to either increase, decrease, or remain unchanged after March 19. An exponential prior with mean 1.0 was used for the initial size of the E class. The I_l and I_h were assumed to be negligibly small at the beginning of the *SEIR* dynamics. The PhyDyn t_0 parameter was set to 2019.7 and a constant population size coalescent model was used prior to this date when proposed trees had earlier root dates. *SEIR* dynamics were assumed to begin on February 1st. Sequences sampled from Israel were randomly assigned to I_h with probability p_h and to I_l with probability $1 - p_h$. XML files to run both BEAST2 and PhyDyn were generated using a custom Python 3 script which was designed to edit a template XML file originally generated with BEAUti and manually edited. MCMC chains for each parameter set were run for at least 1.9 million steps. Convergence was assessed based on visual inspection of parameter traces. Longer MCMC chains and additional replicates are currently being conducted. The first 50% of MCMC steps were discarded as burn-in. BEAST2 log and tree files were combined using LogCombiner. Maximum clade credibility trees were generated using TreeAnnotator. BEAST2 and PhyDyn outputs were visualized using Python 3, Matplotlib (Hunter 2007), Seaborn, and Baltic (https://github.com/evogytis/baltic).

Data and code availability

The assembled SARS-CoV-2 genomes (consensus sequences) were uploaded to GISAID (Table S1). Submission of the raw sequencing data to Sequence Read Archive (SRA) is pending. Code for phylodynamic analysis and model XML configuration, as well as scripts to analyze outputs are available at: https://github.com/SternLabTAU/SARSCOV2NGS.

Acknowledgements

We wish to thank Dr. Boaz Lev at the Israeli Ministry of Health and Dr. Tal Katz-Ezov at the Technion Genome Center, as well as Stern lab members for their support during an ongoing pandemic and various stages of lockdown. This work was funded by the Israeli Science Foundation (1333/16) and by a generous donation from the Milner foundation and from AppFlyer. This study was supported in part by a fellowship to DM, TK and OT from the Edmond J. Safra Center for Bioinformatics at Tel-Aviv University.

medRxiv preprint doi: https://doi.org/10.1101/2020.05.21.20104521.this version posted May 22, 2020. The copyright holder for this preprint (which was not certified by peer review) is the author/funder, who has granted medRxiv a license to display the preprint in perpetuity. It is made available under a CC-BY-NC-ND 4.0 International license .

References

Geneva: World Health Organization. Coronavirus disease 2019 (COVID-19): situation report — 51. In. (https://www .who.int/ docs/ default -source/coronaviruse/situation - reports/20200311 -sitrep-51-covid-19.pdf.

Altschul SF, Madden TL, Schaffer AA, Zhang J, Zhang Z, Miller W, Lipman DJ. 1997. Gapped BLAST and PSI-BLAST: a new generation of protein database search programs. Nucleic Acids Research 25:3389.

Armstrong GL, MacCannell DR, Taylor J, Carleton HA, Neuhaus EB, Bradbury RS, Posey JE, Gwinn M. 2019. Pathogen Genomics in Public Health. New England Journal of Medicine 381:2569-2580.

Bedford T, Greninger AL, Roychoudhury P, Starita LM, Famulare M, Huang M-L, Nalla A, Pepper G, Reinhardt A, Xie H, et al. 2020. Cryptic transmission of SARS-CoV-2 in Washington State. medRxiv:2020.2004.2002.20051417.

Bi Q, Wu Y, Mei S, Ye C, Zou X, Zhang Z, Liu X, Wei L, Truelove SA, Zhang T, et al. 2020. Epidemiology and transmission of COVID-19 in 391 cases and 1286 of their close contacts in Shenzhen, China: a retrospective cohort study. The Lancet Infectious Diseases.

Bouckaert R, Vaughan TG, Barido-Sottani J, Duchene S, Fourment M, Gavryushkina A, Heled J, Jones G, Kuhnert D, De Maio N, et al. 2019. BEAST 2.5: An advanced software platform for Bayesian evolutionary analysis. Plos Computational Biology 15.

Chinazzi M, Davis JT, Ajelli M, Gioannini C, Litvinova M, Merler S, Pastore YPA, Mu K, Rossi L, Sun K, et al. 2020. The effect of travel restrictions on the spread of the 2019 novel coronavirus (COVID-19) outbreak. Science 368:395-400.

Danesh G, Elie B, Alizon S. 2020. Early phylodynamics analysis of the COVID-19 epidemics in France. http://virological.org/t/early-phylodynamics-analysis-of-the-covid-19-epidemics-in-france-using-194-genomes-april-10-2020/467.

Endo A, Group CftMMoIDC-W, Abbott S, Kucharski A, Funk S. 2020. Estimating the overdispersion in COVID-19 transmission using outbreak sizes outside China Wellcome Open Res 5:67.

Fauver JR, Petrone ME, Hodcroft EB, Shioda K, Ehrlich HY, Watts AG, Vogels CBF, Brito AF, Alpert T, Muyombwe A, et al. 2020. Coast-to-Coast Spread of SARS-CoV-2 during the Early Epidemic in the United States. Cell.

Flaxman S, Mishra S, Gandy A, al. e. 2020. Estimating the number of infections and the impact of nonpharmaceutical interventions on COVID-19 in 11 European countries. Imperial College London doi: https://doi.org/10.25561/77731.

Gardy JL, Loman NJ. 2018. Towards a genomics-informed, real-time, global pathogen surveillance system. Nat Rev Genet 19:9-20.

Gelbart M, Harari S, Ben-Ari Ya, Kustin T, Wolf D, Mandelboim M, Mor O, Pennings P, Stern A. 2019. Accurate in vivo population sequencing uncovers drivers of within-host genetic diversity in viruses. bioRxiv:349498.

medRxiv preprint doi: https://doi.org/10.1101/2020.05.21.20104521.this version posted May 22, 2020. The copyright holder for this preprint (which was not certified by peer review) is the author/funder, who has granted medRxiv a license to display the preprint in perpetuity. It is made available under a CC-BY-NC-ND 4.0 International license .

Hadfield J, Brito AF, Swetnam DM, Vogels CBF, Tokarz RE, Andersen KG, Smith RC, Bedford T, Grubaugh ND. 2019. Twenty years of West Nile virus spread and evolution in the Americas visualized by Nextstrain. PLoS Pathog 15.

Hadfield J, Megill C, Bell SM, Huddleston J, Potter B, Callender C, Sagulenko P, Bedford T, Neher RA. 2018. Nextstrain: real-time tracking of pathogen evolution. Bioinformatics 34:4121-4123.

He X, Lau EHY, Wu P, Deng X, Wang J, Hao X, Lau YC, Wong JY, Guan Y, Tan X, et al. 2020. Temporal dynamics in viral shedding and transmissibility of COVID-19. Nat Med.

Holland LA, Kaelin EA, Maqsood R, Estifanos B, Wu LI, Varsani A, Halden RU, Hogue BG, Scotch M, Lim ES. 2020. An 81 base-pair deletion in SARS-CoV-2 ORF7a identified from sentinel surveillance in Arizona (Jan-Mar 2020). medRxiv:2020.2004.2017.20069641.

Huang C, Wang Y, Li X. 2020. Clinical features of patients infected with 2019 novel coronavirus in Wuhan, China (vol 395, pg 497, 2020). Lancet 395:496-496.

Hunter JD. 2007. Matplotlib: A 2D Graphics Environment. Computing in Science & Engineering 9:90-95.

Kendall M, Colijn C. 2016. Mapping Phylogenetic Trees to Reveal Distinct Patterns of Evolution. Molecular Biology and Evolution 33:2735-2743.

Khoury MJ, Bowen MS, Clyne M, Dotson WD, Gwinn ML, Green RF, Kolor K, Rodriguez JL, Wulf A, Yu W. 2018. From public health genomics to precision public health: a 20-year journey. Genetics in Medicine 20:574-582.

Kissler SM, Tedijanto C, Goldstein E, Grad YH, Lipsitch M. 2020. Projecting the transmission dynamics of SARS-CoV-2 through the postpandemic period. Science:eabb5793.

Korber B, Fischer W, Gnanakaran S, Yoon H, Theiler J, Abfalterer W, Foley B, Giorgi E, Bhattacharya T, Parker M, et al. 2020. Spike mutation pipeline reveals the emergence of a more transmissible form of SARS-CoV-2. bioRxiv:2020.2004.2029.069054.

Lloyd-Smith JO, Schreiber SJ, Kopp PE, Getz WM. 2005. Superspreading and the effect of individual variation on disease emergence. Nature 438:355-359.

Menachery VD, Debbink K, Baric RS. 2014. Coronavirus non-structural protein 16: Evasion, attenuation, and possible treatments. Virus Research 194:191-199.

Nguyen LT, Schmidt HA, von Haeseler A, Minh BQ. 2015. IQ-TREE: A Fast and Effective Stochastic Algorithm for Estimating Maximum-Likelihood Phylogenies. Molecular Biology and Evolution 32:268-274.

Sagulenko P, Puller V, Neher RA. 2018. TreeTime: Maximum-likelihood phylodynamic analysis. Virus Evolution 4.

Su YC, Anderson DE, Young BE, Zhu F, Linster M, Kalimuddin S, Low JG, Yan Z, Jayakumar J, Sun L, et al. 2020. Discovery of a 382-nt deletion during the early evolution of SARS-CoV-2. bioRxiv:2020.2003.2011.987222.

medRxiv preprint doi: https://doi.org/10.1101/2020.05.21.20104521.this version posted May 22, 2020. The copyright holder for this preprint (which was not certified by peer review) is the author/funder, who has granted medRxiv a license to display the preprint in perpetuity. It is made available under a CC-BY-NC-ND 4.0 International license .

Tian H, Liu Y, Li Y, Wu CH, Chen B, Kraemer MUG, Li B, Cai J, Xu B, Yang Q, et al. 2020. An investigation of transmission control measures during the first 50 days of the COVID-19 epidemic in China. Science.

Vaughan TG, Nadeau S, Scire J, Stadler T. 2020. Phylodynamic Analyses of outbreaks in China, Italy, Washington State (USA), and the Diamond Princess. http://virological.org/t/phylodynamic-analyses-of-outbreaks-in-china-italy-washington-state-usa-and-the-diamond-princess/439.

Volz E. 2020. http://sarscov2phylodynamics.org.

Volz E, Baguelin M, Bhatia S, Boonyasiri A, al. e. 2020. Report 5: Phylogenetic analysis of SARS-CoV-2. https://www.imperial.ac.uk/media/imperial-college/medicine/mrc-gida/2020-02-15-COVID19-Report-5.pdf.

Volz E, Boyd O, Geidelberg L, Jorgensen D, Ragonnet M, Siveroni I, Team" ICC-R. 2020. Time of epidemic seeding events.

Volz EM. 2012. Complex Population Dynamics and the Coalescent Under Neutrality. Genetics 190:187-U311.

Volz EM, Koelle K, Bedford T. 2013. Viral phylodynamics. PLoS Comput Biol 9:e1002947.

Volz EM, Siveroni I. 2018. Bayesian phylodynamic inference with complex models. PLoS Comput Biol 14:e1006546.

Yu GC, Smith DK, Zhu HC, Guan Y, Lam TTY. 2017. GGTREE: an R package for visualization and annotation of phylogenetic trees with their covariates and other associated data. Methods in Ecology and Evolution 8:28-36.

Zhang X, Shao Y, Tian J, Liao Y, Li P, Zhang Y, Chen J, Li Z. 2019. pTrimmer: An efficient tool to trim primers of multiplex deep sequencing data. BMC Bioinformatics 20:236.

Zhou P, Yang XL, Wang XG, Hu B, Zhang L, Zhang W, Si HR, Zhu Y, Li B, Huang CL, et al. 2020. A pneumonia outbreak associated with a new coronavirus of probable bat origin. Nature 579:270-+.

Zhu N, Zhang DY, Wang WL, Li XW, Yang B, Song JD, Zhao X, Huang BY, Shi WF, Lu RJ, et al. 2020. A Novel Coronavirus from Patients with Pneumonia in China, 2019. New England Journal of Medicine 382:727-733.

medRxiv preprint doi: https://doi.org/10.1101/2020.05.21.20104521.this version posted May 22, 2020. The copyright holder for this preprint (which was not certified by peer review) is the author/funder, who has granted medRxiv a license to display the preprint in perpetuity. It is made available under a CC-BY-NC-ND 4.0 International license .

Table S1. Details of samples sequenced.

Sample ID	Ct E	Ct RdRp	Ct N	Ct average	Sex	Age	Date	Hospital	Genome coverage	Geog. location of sample
1639953	28.5	30.5	32	30.18	M	10-19	26/3/20	Poria	0.996	North
1639996	23.1	24.4	26	24.45	M	20-29	26/3/20	Poria	0.996	North
2020038	22.5			22.46	F	50-59	17/3/20	Hadassah	0.994	Tel Aviv
2020051	30.9			30.87	M	40-49	17/3/20	Hadassah	0.976	Tel Aviv
2020063	28.4			28.39	F	20-29	17/3/20	Hadassah	0.985	Jerusalem
2020068	24.8			24.78	F	20-29	17/3/20	Hadassah	0.986	Jerusalem
2020069	28.2			28.24	F	30-39	17/3/20	Hadassah	0.987	Jerusalem
2020078	21.5			21.5	M	50-59	17/3/20	Hadassah	0.989	Jerusalem
2020084	24.9			24.87	M	60-69	17/3/20	Hadassah	0.994	Jerusalem
2020087	21.5			21.48	M	20-29	17/3/20	Hadassah	0.996	Jerusalem
2023920	18.6			18.56	M	40-49	17/3/20	Hadassah	0.996	Jerusalem
2023922	28			28	F	20-29	17/3/20	Hadassah	0.979	Jerusalem
2046129	23.1	24.2	27	24.88	M	20-29	31/3/20	Poria	0.996	North
2046171	29.6	30.8	33	31.24	F	50-59	31/3/20	Poria	0.954	North
2046434	19.5	20.6	24	21.28	F	50-59	1/4/20	Poria	0.996	North
2046548	28.5	31.1	34	31.01	M	40-49	1/4/20	Poria	0.991	North
2046614	24.4	26.2	28	26.24	F	30-39	2/4/20	Poria	0.996	North
2046616	20.5	22.3	25	22.47	F	70-79	2/4/20	Poria	0.996	North
2046815	13.8	16.5	18	16.08	F	80-89	4/4/20	Poria	0.994	North
2047004	23	24.5	27	24.81	M	30-39	27/3/20	Poria	0.996	North
2047011	28.5	30.2	32	30.24	M	20-29	26/3/20	Poria	0.952	North
2047016	25.7	26.7	29	26.99	F	0-9	26/3/20	Poria	0.996	North
2047145	10.3	11.8	15	12.38	F	30-39	26/3/20	Poria	0.996	North
2047188	13.6	15.3	18	15.48	M	20-29	26/3/20	Poria	0.996	North
2047189	9.75	11.7	14	11.87	M	20-29	26/3/20	Poria	0.996	North
2047364	20.8	22.8	25	22.68	F	60-69	28/3/20	Poria	0.996	North
2047392	27.6	29.9	31	29.42	F	30-39	29/3/20	Poria	0.966	North
2047418	24	25.4	28	25.67	M	0-9	29/3/20	Poria	0.996	North
2047567	26.8	28.7	31	28.97	F	30-39	29/3/20	Poria	0.978	North
2047586	22.8	24.1	27	24.71	F	20-29	29/3/20	Poria	0.996	North
2047604	22.7	24	26	24.32	M	50-59	29/3/20	Poria	0.996	North
2047738	20	22.1	25	22.21	M	10-19	30/3/20	Poria	0.996	North
2047749	19.3	20.7	23	21.03	F	40-49	30/3/20	Poria	0.996	North
2047772	23.8	25.7	26	25.3	F	30-39	30/3/20	Poria	0.996	North
2047883	21.1	22.9	25	22.87	M	60-69	31/3/20	Poria	0.996	North
2047927	32	33.7	36	33.74	F	60-69	31/3/20	Poria	0.918	North
2086001	28.4			28.4	F	10-19	1/4/20	Hadassah	0.988	Jerusalem
2086004	24.6			24.63	F	20-29	1/4/20	Hadassah	0.993	Jerusalem
2086008	20.2			20.24	M	90+	1/4/20	Hadassah	0.996	Jerusalem
2086012	24.4			24.39	M	20-29	1/4/20	Hadassah	0.988	Jerusalem
2086022	27.9			27.88	M	20-29	1/4/20	Hadassah	0.986	Jerusalem
2086033	28.8			28.79	F	60-69	1/4/20	Hadassah	0.991	Jerusalem
2086034	30			30.01	F	20-29	1/4/20	Hadassah	0.981	Jerusalem
2086045	20			19.99	M	50-59	1/4/20	Hadassah	0.996	Jerusalem

medRxiv preprint doi: https://doi.org/10.1101/2020.05.21.20104521.this version posted May 22, 2020. The copyright holder for this preprint (which was not certified by peer review) is the author/funder, who has granted medRxiv a license to display the preprint in perpetuity. It is made available under a CC-BY-NC-ND 4.0 International license .

2089366	20.4			20.36	M	20-29	1/4/20	Hadassah	0.996	Jerusalem
2089368	25.6			25.62	M	60-69	1/4/20	Hadassah	0.985	Jerusalem
2089375	27.5			27.54	M	10-19	1/4/20	Hadassah	0.992	Jerusalem
2089380	30.1			30.14	F	60-69	1/4/20	Hadassah	0.979	Jerusalem
2089383	29.8			29.79	M	30-39	1/4/20	Hadassah	0.989	Jerusalem
2089697	28.3			28.27	F	20-29	1/4/20	Hadassah	0.989	Jerusalem
2089698	28.6			28.58	F	50-59	1/4/20	Hadassah	0.984	Jerusalem
2089712	25.5			25.52	M	20-29	1/4/20	Hadassah	0.989	Jerusalem
2089718	20.6			20.6	F	30-39	1/4/20	Hadassah	0.996	Jerusalem
2089723	28.6			28.55	M	30-39	1/4/20	Hadassah	0.992	Jerusalem
2089812	23.3			23.29	F	20-29	1/4/20	Hadassah	0.995	Jerusalem
2089839	25.5			25.5	M	60-69	1/4/20	Hadassah	0.989	Jerusalem
2089852	25.5			25.53	F	60-69	1/4/20	Hadassah	0.989	Jerusalem
2089861	18.3			18.31	M	70-79	1/4/20	Hadassah	0.996	Jerusalem
2089863	18.8			18.8	M	30-39	1/4/20	Hadassah	0.996	Jerusalem
2089866	20.7			20.7	M	30-39	1/4/20	Hadassah	0.996	Jerusalem
2099018	30.3			30.34	F	60-69	2/4/20	Hadassah	0.980	Jerusalem
2099019	27.5			27.48	M	20-29	2/4/20	Hadassah	0.992	Jerusalem
2099159	27.3			27.3	F	10-19	2/4/20	Hadassah	0.988	Jerusalem
2099251	23			22.98	F	20-29	2/4/20	Hadassah	0.996	Jerusalem
2099416	29			28.98	M	20-29	2/4/20	Hadassah	0.983	Jerusalem
2099421	20.5			20.45	M	50-59	2/4/20	Hadassah	0.996	Jerusalem
2107132	29.9			29.91	F	50-59	14/4/20	Hadassah	0.996	Jerusalem
2107137	19.6			19.6	F	10-19	14/4/20	Hadassah	0.996	Jerusalem
2107681	22.3			22.3	F	30-39	14/4/20	Hadassah	0.996	Jerusalem
2113155	25.6			25.55	M	0-9	15/4/20	Hadassah	0.996	Jerusalem
2113161	25.9			25.92	M	70-79	15/4/20	Hadassah	0.996	Jerusalem
2113173	29.8			29.78	M	10-19	15/4/20	Hadassah	0.996	Jerusalem
2113174	26.4			26.42	M	70-79	15/4/20	Hadassah	0.996	Tel Aviv
2113178	26.6			26.62	M	20-29	15/4/20	Hadassah	0.996	Jerusalem
2113255	29.1			29.14	F	60-69	14/4/20	Hadassah	0.994	Jerusalem
2113256	29.7			29.65	F	10-19	14/4/20	Hadassah	0.996	Jerusalem
2113601	25.1			25.07	M	0-9	15/4/20	Hadassah	0.996	Jerusalem
2113603	21.7			21.72	M	70-79	15/4/20	Hadassah	0.996	Jerusalem
2113678	29.8			29.78	M	0-9	15/4/20	Hadassah	0.996	Tel Aviv
2115701	26			25.96	F	10-19	16/4/20	Hadassah	0.996	Jerusalem
2115964	28.4			28.35	M	10-19	16/4/20	Hadassah	0.996	Tel Aviv
2115968	26.8			26.83	F	20-29	16/4/20	Hadassah	0.996	Tel Aviv
2115976	28.2			28.17	M	60-69	16/4/20	Hadassah	0.985	Tel Aviv
2115980	24.5			24.49	F	20-29	16/4/20	Hadassah	0.912	North
2115990	30.2			30.15	F	50-59	16/4/20	Hadassah	0.996	Jerusalem
2116859	29.6			29.6	F	10-19	20/4/20	Hadassah	0.953	Jerusalem
2123853	28.1			28.05	M	70-79	20/4/20	Hadassah	0.996	Jerusalem
2123863	27.5			27.47	M	80-89	20/4/20	Hadassah	0.996	Jerusalem
13075703	24	25.6	28	25.98	F	20-29	29/3/20	Sheba	0.996	Tel Aviv
13075719	27.7	28.9	31	29.16	F	20-29	29/3/20	Sheba	0.996	Tel Aviv
13075735	26.8	28.4	30	28.47	M	40-49	30/3/20	Sheba	0.996	Tel Aviv
13075782	29.1	30.5	33	30.85	F	40-49	30/3/20	Sheba	0.992	Tel Aviv
13075788	27.8	29.3	31	29.4	F	40-49	30/3/20	Sheba	0.996	Tel Aviv

medRxiv preprint doi: https://doi.org/10.1101/2020.05.21.20104521.this version posted May 22, 2020. The copyright holder for this preprint (which was not certified by peer review) is the author/funder, who has granted medRxiv a license to display the preprint in perpetuity. It is made available under a CC-BY-NC-ND 4.0 International license .

13075790	27.2	28.8	30	28.7	M	50-59	30/3/20	Sheba	0.996	Tel Aviv
13075832	17.5	18.6	20	18.7	M	30-39	30/3/20	Sheba	0.996	Tel Aviv
13075879	18.6	20	22	20.27	M	50-59	30/3/20	Sheba	0.993	Tel Aviv
13075882	18.6	20.4	21	20.1	F	20-29	30/3/20	Sheba	0.996	Tel Aviv
13075914	17.1	18.5	20	18.39	F	50-59	30/3/20	Sheba	0.996	Tel Aviv
13077377	27	29	29	28.33	M	40-49	2/4/20	Sheba	0.996	Tel Aviv
13077383	26	26	28	26.67	F	40-49	2/4/20	Sheba	0.984	Jerusalem
13077413	24	25	26	25	M	70-79	3/4/20	Sheba	0.996	Tel Aviv
13077494	28	29	31	29.33	M	20-29	2/4/20	Sheba	0.856	South Coast
13077497	21	22	24	22.33	F	60-69	2/4/20	Sheba	0.996	South Coast
13077498	17	18	21	18.67	M	20-29	3/4/20	Sheba	0.996	South Coast
13077510	21	22	25	22.67	M	50-59	3/4/20	Sheba	0.993	Jerusalem
13077511	25	26	28	26.33	M	20-29	3/4/20	Sheba	0.986	Jerusalem
13077558	19	20	22	20.33	F	30-39	3/4/20	Sheba	0.996	Tel Aviv
13077560	27	28	30	28.33	F	80-89	3/4/20	Sheba	0.974	Tel Aviv
13077562	15	17	19	17	F	50-59	3/4/20	Sheba	0.988	Tel Aviv
13077564	22	23	25	23.33	F	50-59	3/4/20	Sheba	0.992	Tel Aviv
13077711	27	28	30	28.33	F	30-39	3/4/20	Sheba	0.995	Tel Aviv
13077723	22	23	25	23.33	M	?	3/4/20	Sheba	0.989	Tel Aviv
13077726	20	20	22	20.67	F	60-69	3/4/20	Sheba	0.996	Tel Aviv
13077803	28	29	32	29.67	F	30-39	4/4/20	Sheba	0.981	South Coast
13077823	15	17	19	17	F	10-19	4/4/20	Sheba	0.996	South Coast
13077840	23	25	27	25	M	20-29	4/4/20	Sheba	0.991	Jerusalem
13077846	19	20	23	20.67	F	0-9	4/4/20	Sheba	0.996	Tel Aviv
13077847	24	26	27	25.67	M	10-19	4/4/20	Sheba	0.986	Tel Aviv
13077875	18	19	21	19.33	F	40-49	4/4/20	Sheba	0.996	Tel Aviv
13077882	24	26	27	25.67	M	40-49	4/4/20	Sheba	0.987	Jerusalem
51137031				18.58	M	30-39	1/3/20	Soroka	0.996	Tel Aviv
51137844				27.6	F	30-39	17/3/20	Soroka	0.983	South
51140028				20.56	F	50-59	17/3/20	Soroka	0.996	North
51140068				22.8	M	30-39	18/3/20	Soroka	0.988	South
51140271				28.16	F	40-49	18/3/20	Soroka	0.971	South Coast
51140279				25.76	F	20-29	18/3/20	Soroka	0.976	South Coast
51140315				23.41	M	60-69	18/3/20	Soroka	0.996	South
51140539				19.4	F	50-59	19/3/20	Soroka	0.996	South
51140836				24.5	M	30-39	20/3/20	Soroka	0.986	South
51141014				23.08	F	90+	22/3/20	Soroka	0.996	South
51141121				29.05	M	70-79	22/3/20	Soroka	0.989	South
51141225				18.58	F	40-49	22/3/20	Soroka	0.996	South
51144342				25.59	M	90+	30/3/20	Soroka	0.976	South
51145198				25.49	M	80-89	1/4/20	Soroka	0.989	South
51145482				27.92	F	40-49	5/4/20	Soroka	0.992	Tel Aviv
51146355				29.24	F	80-89	4/4/20	Soroka	0.989	South
51146500				21.79	M	40-49	5/4/20	Soroka	0.989	Tel Aviv
51146503				23.75	F	30-39	5/4/20	Soroka	0.993	Jerusalem
51146669				24.41	M	10-19	5/4/20	Soroka	0.994	Tel Aviv
51146683				24.8	M	10-19	5/4/20	Soroka	0.965	Tel Aviv
130710062	28	28	28	28	M	40-49	14/4/20	Sheba	0.991	Tel Aviv
130710067	23	24	24	23.67	M	60-69	14/4/20	Sheba	0.996	Tel Aviv

medRxiv preprint doi: https://doi.org/10.1101/2020.05.21.20104521.this version posted May 22, 2020. The copyright holder for this preprint (which was not certified by peer review) is the author/funder, who has granted medRxiv a license to display the preprint in perpetuity. It is made available under a CC-BY-NC-ND 4.0 International license .

130710097	29	31	32	30.67	M	70-79	15/4/20	Sheba	0.996	Tel Aviv
130710099	33	33	34	33.33	M	60-69	15/4/20	Sheba	0.979	Tel Aviv
130710157	20	21	24	21.67	M	70-79	15/4/20	Sheba	0.996	Tel Aviv
130710159	27	28	29	28	F	80-89	15/4/20	Sheba	0.990	Tel Aviv
130710211	18	19	20	19	F	70-79	16/4/20	Sheba	0.996	Tel Aviv
130710217	22	23	26	23.67	M	50-59	16/4/20	Sheba	0.996	Tel Aviv
130710390	28	29	30	29	F	30-39	17/4/20	Sheba	0.996	Tel Aviv
130710414	20	21	22	21	M	20-29	17/4/20	Sheba	0.996	Tel Aviv
130710643	31	31	31	31	M	40-49	19/4/20	Sheba	0.986	Tel Aviv
130710644	29	30	31	30	F	80-89	19/4/20	Sheba	0.985	Tel Aviv
130710716	30	31	31	30.67	F	60-69	19/4/20	Sheba	0.989	Tel Aviv
130711082	18.5	20	22	20.17	F	60-69	20/4/20	Sheba	0.996	Tel Aviv
130711104	27	29	29	28.33	F	80-89	20/4/20	Sheba	0.993	Tel Aviv
130711112	31	32	31	31.33	F	80-89	21/4/20	Sheba	0.991	Tel Aviv
130711116	25	27	25	25.67	F	60-69	21/4/20	Sheba	0.996	Tel Aviv
130711367	29	27	27	27.67	F	60-69	22/4/20	Sheba	0.996	North
130711417	32	31	30	31	M	60-69	22/4/20	Sheba	0.974	Tel Aviv
701002313				27	M	50-59	21/3/20	Barzilai	0.996	South Coast
701002314				21	M	20-29	21/3/20	Barzilai	0.996	South Coast
701002317				25	M	50-59	21/3/20	Barzilai	0.996	South Coast
701002327				19	M	50-59	22/3/20	Barzilai	0.996	South Coast
701002334				21	M	70-79	22/3/20	Barzilai	0.996	South Coast
701002403				31	M	40-49	23/3/20	Barzilai	0.996	South Coast
701002407				27	M	40-49	23/3/20	Barzilai	0.959	South Coast
701002426				25	M	60-69	24/3/20	Barzilai	0.996	South Coast
701002431				18	M	20-29	24/3/20	Barzilai	0.996	South Coast
701002440				26	F	20-29	24/3/20	Barzilai	0.996	South Coast
701002442				18	M	30-39	24/3/20	Barzilai	0.996	South Coast
701002455				30	F	20-29	24/3/20	Barzilai	0.992	South Coast
701002456				30	F	60-69	24/3/20	Barzilai	0.980	South Coast
701002458				21	M	40-49	24/3/20	Barzilai	0.996	South Coast
701002462				21	M	70-79	24/3/20	Barzilai	0.996	South Coast
701002489				27	M	40-49	25/3/20	Barzilai	0.996	South Coast
701002504				21	M	70-79	25/3/20	Barzilai	0.996	South Coast
701002538				28	M	70-79	25/3/20	Barzilai	0.996	South Coast
701002540				21	F	40-49	25/3/20	Barzilai	0.996	South Coast
701002550				24	M	30-39	26/3/20	Barzilai	0.996	South Coast
701002555				23	F	40-49	26/3/20	Barzilai	0.996	South Coast
701002556				22	F	60-69	26/3/20	Barzilai	0.996	South Coast
701002561				28	M	50-59	26/3/20	Barzilai	0.996	South Coast
701002591				24	F	50-59	26/3/20	Barzilai	0.996	South Coast
701002666				26	M	40-49	26/3/20	Barzilai	0.996	South Coast
701002681				24	M	60-69	27/3/20	Barzilai	0.996	South Coast
701002752				27	M	10-19	28/3/20	Barzilai	0.987	South Coast
701002768				21	M	50-59	28/3/20	Barzilai	0.996	South Coast
701002786				27	M	60-69	29/3/20	Barzilai	0.996	South Coast
701002792				25	M	50-59	29/3/20	Barzilai	0.995	South Coast
990059202	26.9	28.4	27	27.4	M	60-69	25/3/20	Assuta	0.996	South Coast
990059203	26.5	28.6	27	27.2	F	80-89	25/3/20	Assuta	0.996	South Coast

medRxiv preprint doi: https://doi.org/10.1101/2020.05.21.20104521.this version posted May 22, 2020. The copyright holder for this preprint (which was not certified by peer review) is the author/funder, who has granted medRxiv a license to display the preprint in perpetuity. It is made available under a CC-BY-NC-ND 4.0 International license .

990059204	28.4	30.1	28	28.97	F	30-39	25/3/20	Assuta	0.976	South Coast
990059217	29.1	31.4	32	30.9	M	60-69	25/3/20	Assuta	0.995	South Coast
990059230	26.5	29.7	29	28.5	F	0-9	25/3/20	Assuta	0.972	South Coast
990059231	24.9	28	28	27	M	30-39	25/3/20	Assuta	0.996	South Coast
990059232	24.5	26.7	28	26.3	M	10-19	25/3/20	Assuta	0.996	South Coast
990059233	19.7	21.8	23	21.43	F	50-59	25/3/20	Assuta	0.996	South Coast
990059237	28.3	30.6	32	30.23	F	0-9	25/3/20	Assuta	0.989	South Coast
990059238	24.3	26.3	27	25.83	F	20-29	25/3/20	Assuta	0.996	South Coast
990059244	27.9	30.8	31	29.97	F	?	25/3/20	Assuta	0.938	South Coast
990059251	24.7	28	28	26.9	F	50-59	25/3/20	Assuta	0.996	South Coast
990059252	24.4	26.8	28	26.27	F	20-29	25/3/20	Assuta	0.996	South Coast
990300681	22.9	26.4	27	25.37	F	60-69	30/3/20	Assuta	0.995	South Coast
990300691	29.3	31.7	32	31	M	20-29	31/3/20	Assuta	0.970	South Coast
990300724	23.7	26.6	26	25.53	M	80-89	1/4/20	Assuta	0.993	South Coast
990300860	19.3	21.9	0	20.6	M	20-29	2/4/20	Assuta	0.996	South Coast
990307712	26	27.3	28	26.97	F	20-29	26/3/20	Assuta	0.996	South Coast
990333068	30.1	32.7	34	32.13	M	60-69	24/3/20	Assuta	0.963	South Coast
990333189	29.3	31.4	32	30.9	M	50-59	26/3/20	Assuta	0.950	South Coast
990333193	20.7	22.6	24	22.43	F	40-49	26/3/20	Assuta	0.996	South Coast
990333263	36.4	0	0	36.4	M	30-39	31/3/20	Assuta	0.660	South Coast
990430264	29.3	31.7	33	31.17	F	40-49	29/3/20	Assuta	0.970	South Coast
990430265	29.6	32.2	33	31.7	F	30-39	29/3/20	Assuta	0.994	South Coast

Table S2. Model parameter priors and estimated values

Parameter	Prior	Posterior (Median (95% HPD))						
		p_h = 0.01	p_h = 0.02	p_h = 0.05	p_h = 0.07	p_h = 0.08	p_h = 0.09	p_h = 0.10
Clock rate	Uniform(0.0007, 0.002)	7.7E-4 (7.0E-4, 8.4E-4)	7.3E-4 (7.0E-4, 8.1E-4)	7.4E-4 (7.0E-4, 8.2E-4)	7.5E-4 (7.0E-4, 8.5E-4)	7.8E-4 (7.1E-4, 8.7E-4)	7.5E-4 (7.0E-4, 8.6E-4)	7.5E-4 (7.0E-4, 8.2E-4)
κ	Lognormal(mean = 1.0, sd = 1.25)	3.7 (3.1, 4.5)	3.7 (3.0, 4.4)	3.7 (3.0, 4.4)	3.7 (3.0, 4.5)	3.7 (3.1, 4.5)	3.7 (3.1, 4.5)	3.7 (3.0, 4.3)
γ	Exponential(mean = 1.0)	0.039 (0.003, 0.082)	0.047 (0.003, 0.109)	0.040 (0.002, 0.104)	0.042 (0.003, 0.010)	0.039 (0.002, 0.098)	0.039 (0.005, 0.088)	0.034 (0.003, 0.080)
R_0	Lognormal(mean = 1.5, sd = 0.5)	2.7 (2.5, 2.9)	2.4 (2.3, 2.5)	2.1 (2.0, 2.3)	2.1 (1.9, 2.2)	2.0 (1.9, 2.2)	2.0 (1.9, 2.2)	2.1 (1.9, 2.2)
α	Uniform(0, 2)	0.26 (0.15, 0.49)	0.30 (0.15, 0.51)	0.27 (0.15, 0.49)	0.36 (0.19, 0.63)	0.36 (0.16, 0.66)	0.32 (0.18, 0.58)	0.32 (0.16, 0.65)
E_{init}	Exponential(mean = 1.0)	21 (14, 30)	23 (19, 27)	21 (15, 32)	19 (14, 26)	18 (12, 27)	17 (12, 23)	12 (9, 16)
Y_{init}	Exponential(mean = 1.0)	0.021 (0.018, 0.036)	0.029 (0.029, 0.049)	0.080 (0.026, 0.122)	0.018 (0.012, 0.035)	0.015 (0.012, 0.019)	0.056 (0.040, 0.078)	0.12 (0.07, 0.19)
ρ	Lognormal(mean = 3.6, sd = 1.0)	27 (25, 28)	25 (24, 26)	21 (20, 24)	23 (22, 25)	23 (22, 24)	21 (20, 22)	19 (18, 20)
η	Exponential(mean = 10)	9.4 (6.7, 10.0)	9.7 (8.3, 10.0)	9.5 (7.4, 10.0)	9.5 (7.5, 10.0)	9.2 (6.8, 10.0)	9.5 (7.6, 10.0)	9.7 (8.1, 10.0)